

## Article

# On the Measurability and Predictability of HAZ Softening in GMAW of Automotive DP980 Steel

Cecilio J. Martínez-González <sup>1</sup>, Enrique A. López-Baltazar <sup>1,\*</sup>, Francisco Alvarado-Hernández <sup>1</sup>, Víctor H. Baltazar-Hernández <sup>1</sup> , Dulal C. Saha <sup>2</sup> , Elliot Biro <sup>2</sup> and Norman Zhou <sup>2</sup>

<sup>1</sup> Materials Science and Engineering Program, Universidad Autónoma de Zacatecas, Zacatecas 98000, Mexico; cecilio.jmartinezg@uaz.edu.mx (C.J.M.-G.); ingenierofah@uaz.edu.mx (F.A.-H.); victor.baltazar@uaz.edu.mx (V.H.B.-H.)

<sup>2</sup> Centre for Advanced Materials Joining, University of Waterloo, Waterloo, ON N2L 3G1, Canada; dcsaha@uwaterloo.ca (D.C.S.); ebiro@uwaterloo.ca (E.B.); nzhou@uwaterloo.ca (N.Z.)

\* Correspondence: ealopezb@uaz.edu.mx

**Abstract:** Dual Phase (DP) steel, composed of a ferrite matrix with dispersed islands of martensite, has become popular in auto-body car construction due to its outstanding mechanical properties (i.e., high strength and good ductility). DP steel softens at the sub-critical heat-affected zone (SC-HAZ) when subjected to welding thermal cycles, owing to the tempering of the martensite phase. In this work, DP980 steel was subjected to varied thermal cycles: (a) furnace-tempering treatment, (b) gas metal arc welding (GMAW), and (c) resistance spot welding (RSW), in order to characterize the tempering of martensite below the  $A_{c1}$  critical temperature and at the sub-critical heat-affected zone (SC-HAZ) in the case of the welded specimens. The coarsening stage of cementite phase was characterized through microstructure observations and hardness measurements. As expected, the comparative results indicated an advanced stage of the martensite tempering in the furnace heat-treated specimens, followed by the GMAW and the RSW specimens. Further, developed softening kinetic models have been suitably employed and adjusted in order to predict the extent of softening along the SC-HAZ of the GMAW specimen. Finally, as the advanced stage of cementite coarsening is due to the influence of the arc welded thermal cycle, a reasonable estimation of the hardness profile was obtained, particularly for tempering temperatures above 400 °C.

**Keywords:** DP980 steel; GMAW; heat-affected zone; tempering; softening kinetics



**Citation:** Martínez-González, C.J.; López-Baltazar, E.A.; Alvarado-Hernández, F.; Baltazar-Hernández, V.H.; Saha, D.C.; Biro, E.; Zhou, N. On the Measurability and Predictability of HAZ Softening in GMAW of Automotive DP980 Steel. *Metals* **2022**, *12*, 1009. <https://doi.org/10.3390/met12061009>

Academic Editor: João Pedro Oliveira

Received: 17 May 2022

Accepted: 10 June 2022

Published: 14 June 2022

**Publisher's Note:** MDPI stays neutral with regard to jurisdictional claims in published maps and institutional affiliations.



**Copyright:** © 2022 by the authors. Licensee MDPI, Basel, Switzerland. This article is an open access article distributed under the terms and conditions of the Creative Commons Attribution (CC BY) license (<https://creativecommons.org/licenses/by/4.0/>).

## 1. Introduction

To address increasingly stringent regulations regarding occupant safety and air pollution in automobile construction, automakers have successfully introduced dual-phase (DP) steel with several outstanding properties, viz. increased strength and higher energy absorption (vehicle safety) [1]. Meanwhile, vehicle weight reduction through down-gauging is exceptionally advantageous because it favors fuel efficiency and green environmental emissions if employing DP steel [1].

High strength DP steel, with an ultimate tensile strength about 980 MPa (DP980), is composed of ferrite matrix along with a relatively high volume fraction of martensite, ranging from 45 to 55 pct. Softening (reduction of hardness with respect to the base metal) in the sub-critical heat-affected zone (SC-HAZ) due to martensite tempering in DP steels has been widely reported when subjected to different welding processes such as resistance spot welding (RSW) [2–6], laser beam welding (LBW) [7–12], and gas metal arc welding (GMAW) [13–21]. Softening occurring at the SC-HAZ of welded DP steels is predominantly attributed to the tempering of martensite without major influence from the ferrite matrix [22]. In consequence, martensite tempering in DP steel strongly depends on: martensite volume fraction [11], the martensite carbon content, and the alloying level [17,23], and additionally, on the total amount of heat input used in the welding

process [11,13,17]. Then, if comparing the above mentioned welding processes, GMAW logically inputs a greater amount of heat in DP weldments [24]. For instance, it has been reported that the mechanical behavior of DP steel strongly depends on the level of heat input; the higher the heat input (through adjustments in the welding parameters), the higher the tendency to fracture in the softened SC-HAZ [13,15]. Furthermore, other researchers have corroborated that variations in the cooling rate (heat input) lead to differences in the HAZ-softening of DP steel; it has been demonstrated that the lower cooling rate increases the severity of the HAZ-softening [14,17]. These investigations, however, did not provide details on the tempered martensite islands of DP steel subjected to GMAW, in particular by analyzing carbide precipitation and coarsening kinetics. It is worth mentioning that the GMAW process is available for specific purposes when joining DP steels, particularly to join components demanding high load-bearing capacity and/or enhanced fatigue strength such as chassis, suspension parts, reinforcement bars, pillars, among others. Therefore, it is of high relevance to study softening in DP steel when employing arc welding processes.

A methodology to evaluate softening kinetics that could help with predicting the extent of softening along the SC-HAZ has been successfully utilized [25–29]. For instance, Biro et al. employed rapid isothermal tempering through Gleeble simulation (here, rapid isothermal tempering means: fast heating rate i.e., 2190 °C/s, a reasonable holding time at peak temperature, followed by a very rapid cooling rate 4140 °C/s) on various chemistries of DP and martensitic steels. Their investigation suggested that the activation energy derived from the rapid isothermal trials can be used to obtain an equivalent isothermal temperature from the welding thermal cycle, and hence, the maximum HAZ softening can be predicted by employing the Johnson–Mehl–Avrami–Kolmogorov (JMAK) equation [29]. However, in the latter work, the weld temperature history in laser welds was modeled as per the modified Rosenthal’s equation suggested by Xia et al. [11], but no attempts were suggested in order to experimentally validate the weld temperature history at various distances from the fusion line. In other research [26], additional efforts have been made to separate the effects of two main stages of tempering, namely: precipitation and coarsening of cementite (stages I and II respectively), as per Biro et al. [26], that further explained the discrepancy between the activation energy values reported between the conventional and the rapid tempering processes. Thus, derived from these results, it was established that the carbide coarsening kinetic model can be employed in the case of the high heat input welding process (GMAW) and when peak temperatures lie above 420 °C.

Additional analysis is proposed in this work to further evaluate the HAZ softening of GMAW by utilizing the methodology of Biro et al. [25]. Thus, the aim of this research is to characterize the carbide coarsening process in tempered martensite islands of DP980 steel when subjected to varied thermal cycles (i.e., RSW, GMAW, furnace treating) and further employ developed the softening kinetics model in order to predict the extent of softening at the sub-critical heat-affected zone of the GMAW specimens.

It is worth mentioning that the novelty in this research was to demonstrate that approximating the heating cycle as an isothermal cycle (from typical heat-treating furnace data) can result in predictable softening values at the HAZ of the GMAW DP980 steel, which may be used for material characterization.

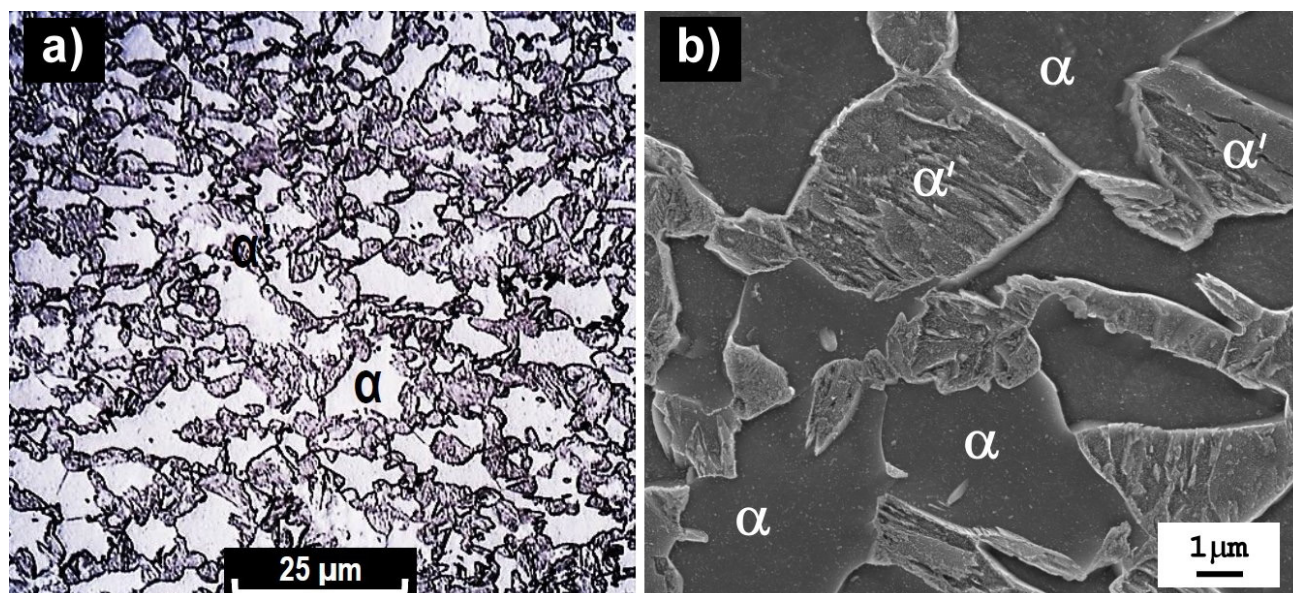
## 2. Materials and Experimental Details

### 2.1. Materials

Galvanized DP980 steel sheet with a thickness of 1.2 mm was used in this work. The chemical composition of the investigated steel is listed in Table 1. The base metal microstructure is composed by a volume fraction of 49 pct. martensite ( $\alpha'$ ) and a ferritic matrix ( $\alpha$ ) as illustrated in Figure 1. The tensile properties provided in Table 2 were obtained experimentally in a universal testing machine Shimadzu AG1 (Shimadzu, Zacatecas, Mexico), based on ASTM E8.

**Table 1.** Chemical composition of DP980 steel sheet (wt.%).

Material	C	Mn	Si	Cu	Ni	Cr	Mo	Nb	V	Al	CE <sub>y</sub>	TA <sub>c1</sub> (°C)
DP980	0.15	1.50	0.31	0.02	0.01	0.02	0.006	0.02	0.003	0.047	0.391	716

**Figure 1.** (a) Base metal microstructure DP980, (b) phase detail ( $\alpha$  = ferrite,  $\alpha'$  = martensite).**Table 2.** Uniaxial tensile properties and hardness of DP980 steel.

Material	YS (MPa)	UTS (MPa)	Elongation (%)	HV
DP980	674	1074	11	342

## 2.2. Tempering Treatments

DP980 steel specimens with dimensions of  $1.2 \times 10 \times 20$  mm (thickness  $\times$  width  $\times$  length) were heat-treated in a muffle furnace at various peak temperatures. Two different tempering paths were performed at maximum temperature of 400, 500, 600 and 700 °C, according to the following: (a) with the purpose of evaluating the effect of isothermal holding on tempering, samples were slow heated ( $\sim 10$  °C/min), plus isothermally holding at maximum temperature for 3600 s, followed by water cooling—this path has been designated as T1-schedule (schematically illustrated in Figure 2a); (b) samples were slow heated ( $\sim 10$  °C/min) up to the maximum temperature and immediately followed by water cooling; this treatment aimed to evaluate the effect of heating path on the tempering and it has been designated as T2-schedule (Figure 2b). The minimum tempering hardness (maximum softening) was obtained from the T1-schedule at 700 °C for 3600 s. Water cooling to room temperature was utilized in order to prevent further alterations after the samples reached the maximum temperature.

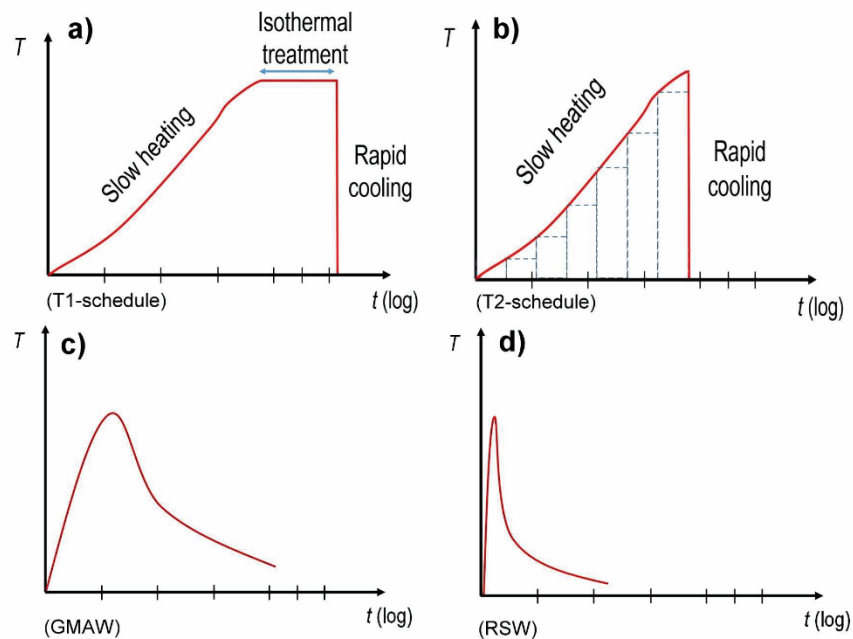


**Figure 2.** Schematic of the thermal cycles applied to DP980 steel: (a) T1-schedule, (b) T2-schedule, (c) GMAW and (d) RSW.

### 2.3. Welding Procedure

GMAW was performed in an Infra<sup>TM</sup> MM 300-E machine (Infra, Zacatecas, Mexico) operated at 10.1 kVA/7.7 kW with non-pulsed short circuit metal transfer mode, using an ER70S-6 solid welding wire of 0.9 mm in diameter, with a travel and work angle of 90°, and by using direct current electrode positive (DCEP). The selected welding parameters are listed in Table 3. The specimens were prepared as 50 mm × 100 mm bead-on-plate coupons. The calculated heat input was 0.403 kJ/mm. Figure 2c depicts a schematic of the GMAW thermal cycle

**Table 3.** Selected welding parameters for GMAW data from [20] and RSW data from [30].

GMAW-Parameter	Current (A)	Voltage (V)	Shield Gas	Gas Flow (L/min)	Travel Speed (mm/s)
	55	16.5	75% CO <sub>2</sub> + 25% Ar	18	1.8
RSW-Parameter	Welding Current (kA)	Force (kN)	Squeeze Time Cycles (s <sup>-1</sup> )	Welding Time Cycles (s <sup>-1</sup> )	Holding Time Cycles (s <sup>-1</sup> )
	9	4.5	25	20	10

With the purpose of measuring the temperature history from GMAW samples, a series of thermocouples were systematically placed at various distances from the fusion line towards the base metal. The experimentally measured welding thermal cycle through thermocouples helped with locating the maximum temperature, and additionally, a minimum number of ten Vickers indentations were performed in such locations of maximum temperature in order to average the local microhardness.

Resistance spot welding (RSW) was additionally performed in this work in order to benchmark the tempering of martensite at the sub-critical heat-affected zone (SC-HAZ) of DP980 steel upon a rapid thermal cycle (i.e., fast heating followed by rapid cooling), therefore, the precipitation and growth of cementite carbides, and the recovery of the lath structure was further compared among the furnace heat-treated specimens, the high heat input welding process (GMAW), and the low heat-input welding process (RSW).

RSW specimens were obtained using a pedestal-type, pneumatically operated machine Robotron series 400 (Ontario, Waterloo, ON, Canada), AC, constant current, 250 kVA

single phase, and 60 Hz frequency, with a pneumatically controlled Centerline Ltd. AC controller to monitor the welding parameters. DAQ system was used with the equipment to monitor the load, displacement, current, and voltage [30]. According to the DP980 steel sheet thickness and the welding force, the employed electrodes were FB25, based on the Resistance Welding Manufacturing Alliance (RWMA) standard [31]. A constant flow water of 4 L/min was maintained for cooling the electrodes, according to AWS standards [32]. RSW parameters are listed in Table 3. In order to estimate the local peak temperature profile at the sub-critical HAZ of DP980 steel (i.e., just beside  $Ac_1$  line), simulations were conducted using commercial finite element software, as detailed in previous work [4] (schematically shown in Figure 2d).

#### 2.4. Microstructure Characterization

Specimens were sectioned across the weldment by covering fusion zone (FZ), heat-affected zone (HAZ), and base metal (BM). Metallographic standard techniques were applied in all cases. Samples for SEM were fine polished with colloidal silica suspension to 0.05  $\mu\text{m}$  all samples were etched with 2 pct. nital solution.

Optical microscopy was carried out in Union Versament-3™ model (Zacatecas, Mexico) and images were processed with Motion Image Plus 2.0™ version 3, Media Cybernetics software (Zacatecas, Mexico). SEM samples were gold-covered and analyzed with a PHILIPS XL30-FEG™ microscope (Ontario, Waterloo, ON, Canada). Microhardness testing was performed at room temperature with 300 g load during 15 s of dwell time by using a microhardness testing machine, Shimadzu HMV-2T™ (Shimadzu, Zacatecas, Mexico); all the indentations were spaced 200  $\mu\text{m}$  apart to avoid the interference in the measurement. Hardness profile was obtained according to sample; for instance, RSW hardness profile was a diagonal line of indentations covering all the weld regions, and GMAW was a line through the weld regions. The tolerances shown in the hardness and carbide dimensions represent the 95-pct. confidence interval.

#### 2.5. Softening Analysis Method

A methodology for assessing softening kinetics has been developed by Biro et al. in previous work [26–28]. On the basis of such analyses,  $\phi$  parameter, which is defined as the fraction of the tempered martensite, was introduced as a reference for rating the degree of tempering; thus, when  $\phi$  equals to one it means that the material is fully tempered, and contrary to this, the material is in its base state if  $\phi$  equals to zero. Parameter  $\phi$  can be calculated as follows:

$$\phi = \frac{H_{base} - H}{H_{base} - H_{Min}} \quad (1)$$

where  $H_{base}$  is the base metal hardness,  $H_{min}$  is the minimum hardness in the material subjected to any specific treatment, and  $H$  is the specimen hardness.

Based on the model developed by Jonhson–Mehl–Avrami–Kolgomorov (JMAK) [28] describing the nucleation, growth and saturation of the transformed product and given by:

$$\phi = 1 - \exp(-kt^n) \quad (2)$$

where  $\phi$  is the fraction of the tempered martensite,  $k$  is the energy barrier for the transformation to occur,  $t$  is the tempering time, and  $n$  is the transformation rate. The fitting parameter  $k$  representing the energy barrier for transformation was modeled by utilizing Arrhenius equation as follows:

$$k = k_0 \exp\left(\frac{-Q}{RT}\right) \quad (3)$$

where  $k_0$  is a fitting parameter, the activation energy for softening is represented by  $Q$ ,  $R$  is the universal gas constant,  $T$  is the temperature.

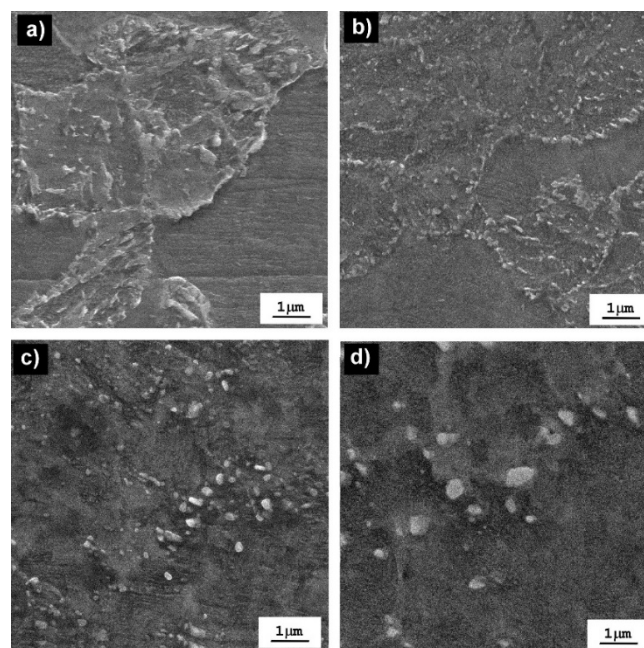
In previous work [27],  $Q$  value was obtained from the  $\phi$  vs.  $t$  plot by fitting the data to Equation (2) by non-linear regression. Thus, the values for  $\phi$  were measured from samples

exposed to isothermal holding at peak temperature in a Gleeble<sup>TM</sup> machine for various  $t$  values. Instead in this work, isothermal intervals are applied during the ramp-up of heating within the furnace at various peak temperatures, as schematically depicted by the horizontal dashed lines in Figure 2b; hence, the values for  $\phi$  are obtained through Equation (1) from the experimentally measured hardness at the peak temperature (at the start of the isothermal transformation) and at the end of the isothermal transformation within the interval (i.e., varied periods of time were taken for the interval from 1 s up to 3600 s). Further, by introducing the various experimentally obtained  $\phi$  within the adequate peak temperature (for example: at 700 °C),  $k$  and  $n$  values were estimated by solving Equation (2). Once  $k$  and  $n$  values are obtained, the activation energy  $Q$  is resolved through Equation (3). The fitting parameter  $k_0 = 0.0028$  was obtained from the linear regression of the plot  $\phi$  vs.  $T$  (°C).

### 3. Results and Discussion

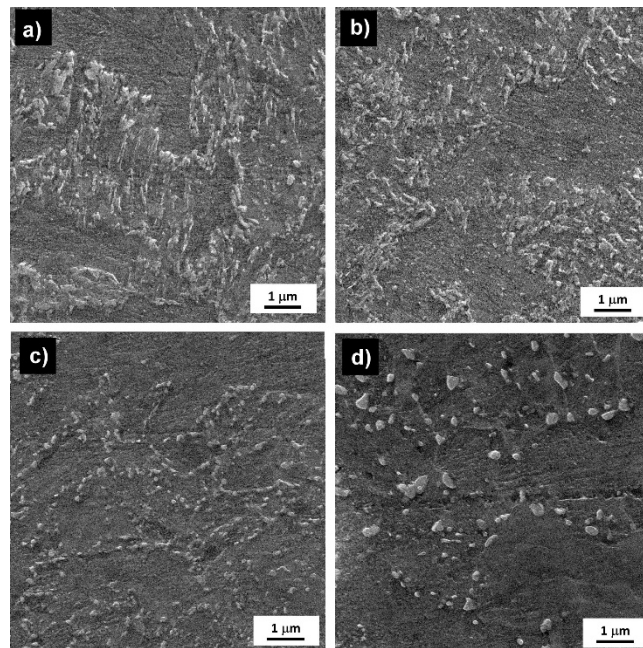
#### 3.1. Microstructure and Hardness

Figure 3 shows the microstructure of the slow-heated plus isothermally tempered DP980 steel for 3600 s of holding time at various peak temperatures: (a) 400 °C, (b) 500 °C, (c) 600 °C, and (d) 700 °C, respectively. Figure 3a indicates that tempered martensite islands ( $\alpha'T$ ) revealed a slightly broken morphology at the grain interior. By further increasing the tempering temperature (i.e., 500~700 °C),  $\alpha'T$  islands morphology kept on changing, as observed in Figure 3b–d; in particular, the microstructure shown in Figure 3d revealed a quite decomposed martensite with a distribution of coarse carbides.



**Figure 3.** Microstructure of the slow-heated and isothermally tempered DP980 steel for 3600 s at the various peak temperatures: (a) 400 °C, (b) 500 °C, (c) 600 °C and, (d) 700 °C. ( $\alpha$  = ferrite,  $\alpha'R$  = tempered martensite).

On the other hand, samples subjected to slow heating followed by rapid cooling resulted in a progressive decomposition of martensite when raising the peak temperature (Figure 4a–d). For instance, the periphery of tempered martensite islands along with a fine distribution of carbides is clearly revealed at 400 °C (Figure 4a), thus contrasting with the barely observable periphery of the tempered martensite island with coarser carbides distributed along the grain boundary. In addition, blocks are still visible in the  $\alpha'T$  containing carbides in all cases of Figure 4.



**Figure 4.** Microstructure of DP980 steel upon slow heating followed by rapid cooling at peak temperatures of: (a) 400 °C, (b) 500 °C, (c) 600 °C, and (d) 700 °C. ( $\alpha$  = ferrite,  $\alpha'$ R = tempered martensite).

Vickers microhardness results listed in Table 4 indicate the degree of softening for both slow-heated conditions plus isothermally tempered or rapidly cooled. A drop of hardness with respect to base metal hardness ( $342 \pm 8$  HV) is seen in all specimens if increasing temperature from 400 °C to 700 °C. It is to be noted that the lowest hardness value logically resulted in the isothermally treated specimen at 700 °C (i.e.,  $166 \pm 6$  HV), which is considered here as fully tempered as further tempering didn't change the microhardness significantly.

**Table 4.** Microhardness results for the different tempering paths.

Temperature (°C)	Slow Heating + Isothermally Treated for 3600 s	Slow Heating + Rapid Cooling
400	$274 \pm 13$	$327 \pm 15$
500	$233 \pm 9$	$302 \pm 13$
600	$207 \pm 3$	$258 \pm 9$
700	$166 \pm 6$	$175 \pm 5$

By comparing the mentioned microstructure and hardness results, there is no doubt that the dominant tempering stage in the low-C DP980 steel martensite is the coarsening of cementite, which is developed during the slow heating process at different peak temperatures. Hence, the isothermal holding at 3600 s is simply the ongoing combined process of coarsening, spheroidizing, and further recovery of ferrite.

As martensite decomposition occurs during heating, the rapid heating involved during the welding process affects softening. Figures 5 and 6 show the hardness profile and the microstructure at the sub-critical heat-affected zone (SC-HAZ) of GMAW and RSW, respectively. Vickers microhardness profile across the weldment for the GMAW condition, provided in Figure 5a along with the path of indentations illustrated in Figure 5b, clearly revealed the extent of softening at the SC-HAZ with a drop in hardness of 157 HV (54% with respect to the BM hardness). The lowest hardness value is marked by "X" (Figure 5a,b) and the corresponding optical micrograph, provided in Figure 5c, revealed a broken morphology of the tempered martensite islands along with finely dispersed presence carbides. Furthermore, Figure 6a,b indicates a drop of hardness of about 60 HV (18%) with respect to the base metal at the SC-HAZ of RSW DP980 steel (located at "X" in Figure 6b).

The periphery of the tempered martensite island along with a slightly broken appearance is clearly observed in Figure 6c. Martensite tempering upon rapid thermal cycles in RSW is clearly less severe if comparing to GMAW.

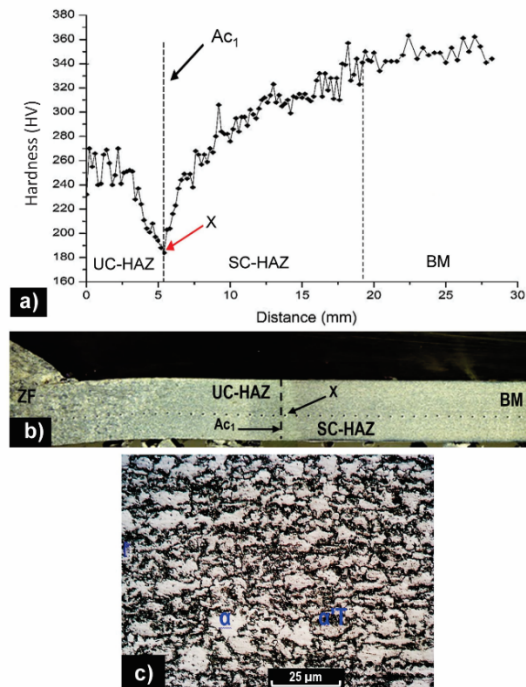


**Figure 5.** DP980 steel subjected to GMAW: (a) microhardness indentations profile across the weldment, (b) weld cross-section showing the sub-critical HAZ, (c) microstructure revealing martensite tempering located just beside the  $Ac_1$  line (obtained from “X”).

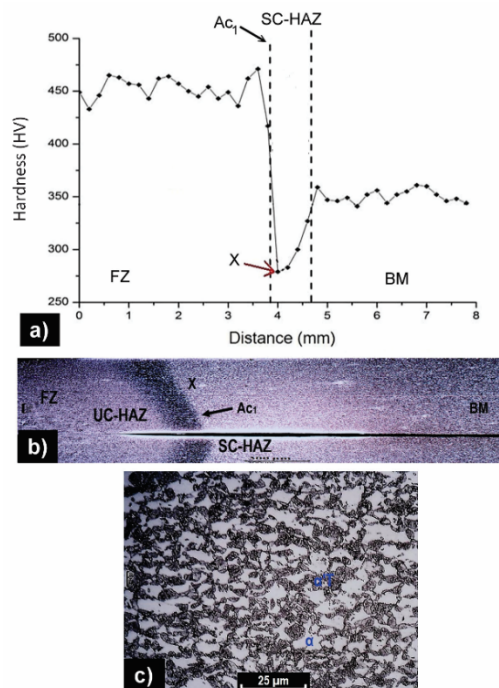


**Figure 6.** Resistance Spot Welding of DP980 steel: (a) microhardness indentations profile across the weldment, (b) weld cross-section showing the sub-critical HAZ, (c) microstructure revealing martensite tempering located just beside the  $Ac_1$  line (obtained from “X”).

To contrast the resultant tempering process at high temperature among previous mentioned conditions, detailed microstructure and large-scale measurements of the actual size of cementite by employing electron microscopy are provided in Figures 7 and 8, respectively. The specimen slow-heated and isothermally treated at 700 °C for 3600 s resulted in the presence of coarse quasi-spherical carbides of cementite ( $405 \pm 52$  nm) preferentially localized at the periphery of the prior austenite grain boundary (Figure 7a). In the structure of the specimens slow-heated up to 700 °C then rapidly cooled, quasi-spherical carbides of cementite had an average size of  $266 \pm 26$  nm and were uniformly distributed within the tempered island of martensite (Figure 7b). It should be noted that the lathe and block morphology of the prior martensite was not observable in this sample. On the other hand, the tempered martensite islands observed at the lowest hardness value at the SC-HAZ of GMAW (Figure 7c) resulted in coarse carbides of cementite ( $147 \pm 23$  nm) evenly distributed within the tempered island. In contrast, Figure 7d clearly revealed the presence of finer carbides (i.e.,  $62 \pm 11$  nm), and some of the prior lathe morphology remained within the tempered island of martensite upon RSW condition.

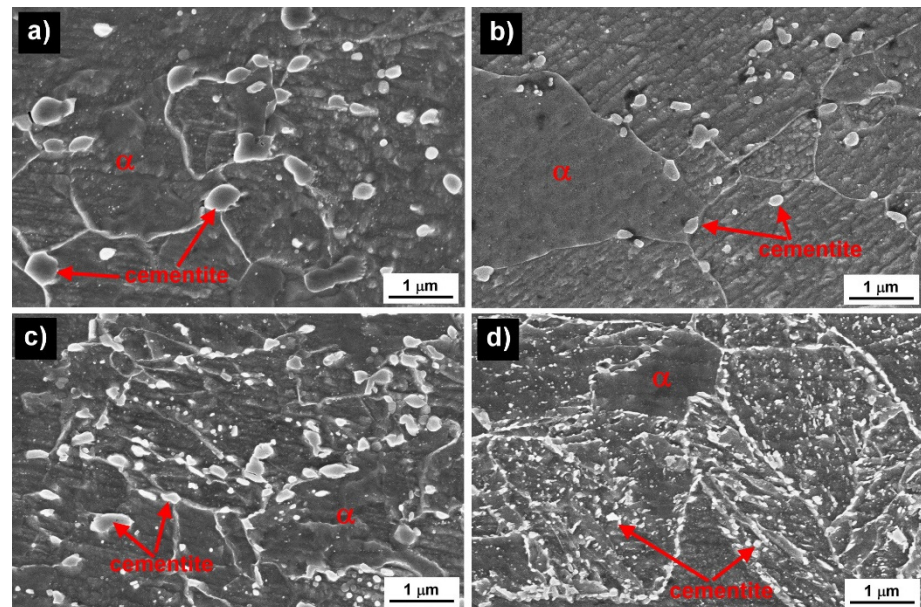


**Figure 7.** Detailed microstructure showing tempering of martensite islands in DP980 steel: (a) slow heating and isothermally treated for 3600 s at 700 °C, (b) slow heating followed by rapid cooling, and rapid tempering obtained from “X” location at the SC-HAZ of (c) GMAW and (d) RSW.

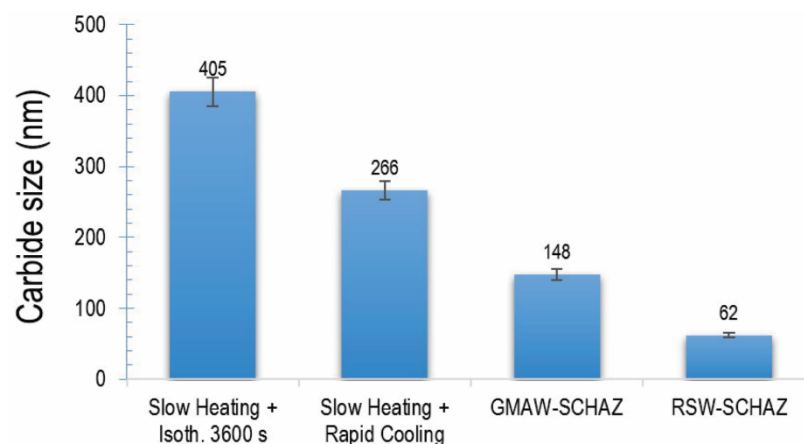


**Figure 8.** Carbid size in tempered martensite islands upon different conditions.

A number of indentations were additionally performed at the SC-HAZ of both GMAW and RSW welds in order to average the minimal hardness. With the averaged hardness values, softening progression  $\phi$  was obtained through Equation (1) as displayed in Figure 9. Based on these results, large-scale softening at the SC-HAZ of GMAW DP steel is observed. Furthermore, it is seen that maximum softening (close to  $A_{c1}$  line) at the SC-HAZ of GMAW welds approaches the resultant value of the specimens slow heated up to 700 °C, followed by rapid cooling specimens. So far, the weld heat input has gone far enough to generate the advanced stage of cementite coarsening at the SC-HAZ of GMAW DP980 steel.

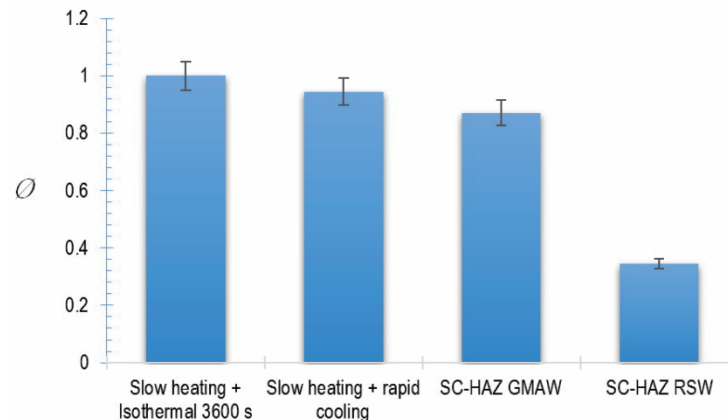


**Figure 9.** Softening progression in tempered martensite islands upon different conditions.

### 3.2. HAZ-Softening Prediction in GMAW of DP980 Steel

Since softening progression data is conveniently used to calculate the activation energy; if solving JMAK equation by utilizing  $\phi$  obtained at 700 °C from selected exposure times, a reasonable value for  $Q = 57$  kJ/mol was calculated from Equation (3) by employing the proposed procedure previously described in the experimental method section. As the exposure time included the ramp-up time where the temperature was variable, it is understood that this value overestimates the actual value of  $Q$  associated with HAZ softening. Such calculated activation energy is quite consistent with values for lean chemistry DP980 steel which ranged 39~54 kJ/mol from previous work [27], which shows that approximating the heating cycle as an isothermal cycle can result in reasonable softening values that might be used for material characterization without the use of a complex apparatus (such as a Gleeble) that is not universally accessible. Recall that coarsening of cementite particles is the predominant process occurring within the range of temperature 400~700 °C [26]; hence, the calculated  $Q$  value here is utilized for further calculations.

When attempting to calculate  $\phi$  value from the Equation (1) for the complete range of temperature 400 °C–700 °C; it was not possible to adjust into Equation (2) owe to the long time exposure during the heating path. The transformation rate obtained ( $n \sim 0.00788$ ), corresponded well with the process of the cementite coarsening during the slow heating path, and additionally the low  $k$  value indicated a high energy barrier. As a consequence, it takes more time and makes it relatively difficult initiate softening [28].

In order to overcome the above mentioned problem when calculating the energy barrier for the long time exposure; short isothermal heating cycles were ideally assumed during the heating path (10 °C/min) at various peak temperature and time (as illustrated schematically by the dashed lines in Figure 2b) in the slow heating followed by rapid cooling specimens; then it was possible to estimate  $\phi$  value from Equation (2), for instance, at the lower peak temperature (i.e., 400 °C) and the corresponding higher temperature (i.e., 500 °C), and so on. By going further, a comparison between the calculated and experimental hardness values was obtained for the assessed range of temperatures; as a result, acceptable correspondence ( $\pm 9$  HV) between the predicted and the experimental hardness is revealed in Figure 10.

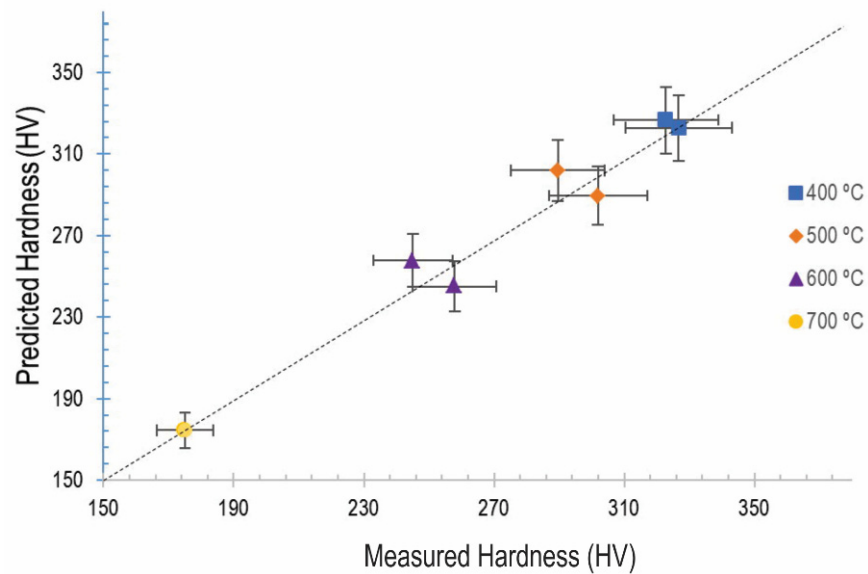


**Figure 10.** Comparison between the measured and the predicted hardness by the JMAK equation from the slow heating followed by rapid cooling condition.

On the other hand, a series of trials employing thermocouples were conducted in order to obtain the peak temperatures and corresponding local hardness at various distances through the SC-HAZ and towards the base metal in gas metal arc welded DP980 steel. According to Figure 11, the measured peak temperatures and their corresponding local hardness values agreed well with the hardness predicted by employing the JMAK equation ( $\pm 11$  HV) in the slow-heated and rapidly cooled specimens, which is represented by an exponential relationship.

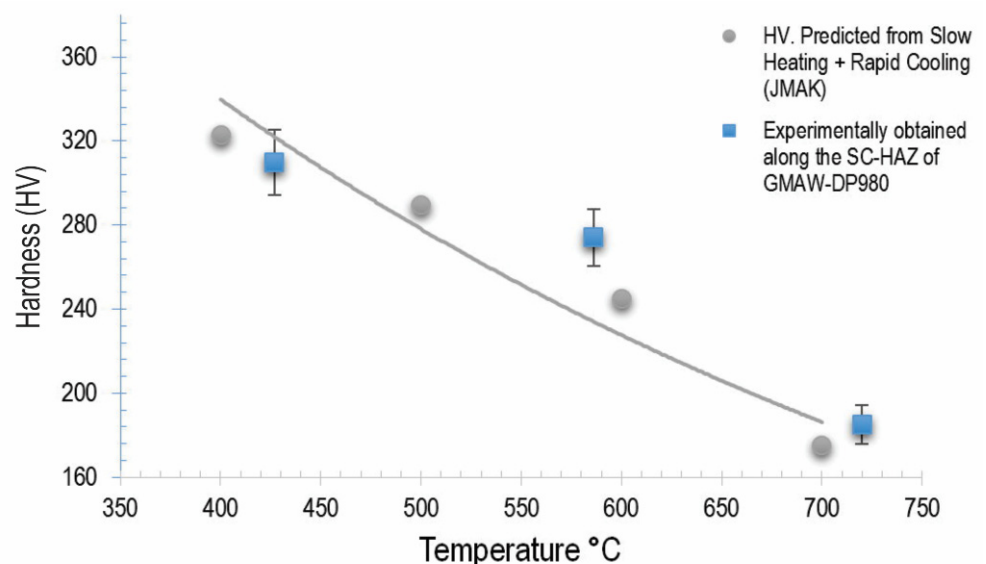


**Figure 11.** Comparison between the predicted hardness and the measured hardness at specific locations along SC-HAZ of GMAW DP980 steel.

As other authors cited in the earlier work [27], it was assumed that in the thermal history during welding, the temperature history behaves nearly parabolically, particularly with a tempering temperature equal to the alloy  $A_{c1}$  temperature (Table 1). Then, by

equating Equation (2) evaluated at alloy  $Ac_1$  temperature to Equation (2) evaluated at SC-HAZ temperature during the welding, the following expression [27] could be used:

$$t_{loc} = \int_{t=0}^{t=2\tau} \exp \left[ \frac{Q}{Rn} \left( \frac{1}{T_{loc}} - \frac{1}{T} \right) \right] dt \quad (4)$$

where  $t_{loc}$  is the equivalent isothermal tempering time at the desired location along the SC-HAZ,  $Q$  is the activation energy,  $n$  is the time exponent,  $R$  is the universal gas constant,  $T$  is the ambient temperature and  $T_{loc}$  is the temperature at the desired location. Once the isothermal tempering time is calculated then the extent of softening along the SC-HAZ of GMAW DP980 steel can be predicted again by applying Equation (2).

To predict the entire hardness in the upper critical heat-affected zone (UC-HAZ), the hardness profile was modeling using Yurioka's model [33]:

$$Hv = \frac{H_M + H_B}{2} - \frac{H_M - H_B}{2.20} \arctan \left[ 4 \frac{\log \frac{t_{8/5}}{t_M}}{\log \frac{t_B}{t_M}} - 2 \right] \quad (5)$$

where  $H_M$  is the hardness of a fully martensitic structure,  $H_B$  is the hardness of a fully bainitic structure, both depending on the material chemistry. The time for the material to cool from 800 °C to 500 °C is given by  $t_{8/5}$ ,  $t_M$  is the maximum time to produce a fully martensitic structure, and  $t_B$  is the minimum time to produce a non-martensitic structure, all the abovementioned relations are properly detailed in [33].

In Figure 12, the predicted hardness has been superimposed on the actual hardness profile of GMAW DP980 steel along the HAZ. The predicted hardness profile using the JAMK equation under-predicts the hardness profile, particularly at a high temperature close to  $Ac_1$  (approximately at 700 °C); this result can be explained in terms of the tempering progression of the slow-heated specimen and the SC-HAZ of GMAW. In both conditions, the coarsening of cementite stage is developed at high temperature; however, the tempering progression is further delayed at the SC-HAZ according to the microstructure in Figure 7, thus resulting in a smaller carbide size and greater hardness.

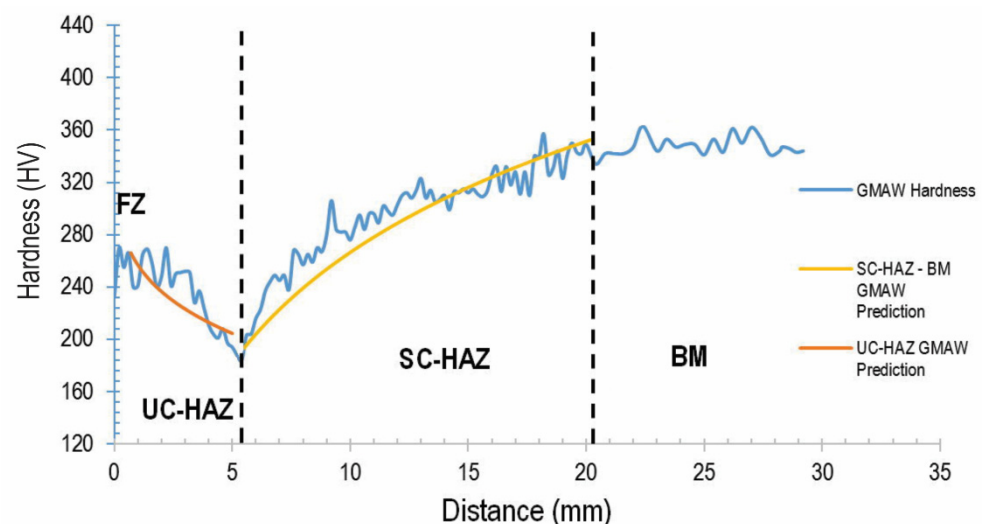


**Figure 12.** Hardness prediction along the HAZ of GMAW DP980 steel.

Although the above-developed process could have introduced errors, particularly when assuming short isothermals during the heating path, it seems that the short tempering time taken for calculations lead us to obtain a reasonable correspondence if attempting to predict the extension of softening along the SC-HAZ of GMAW DP980.

#### 4. Conclusions

1. Tempered martensite islands in the SC-HAZ of GMAW DP980 steel containing coarse cementite carbides of approximately  $147 \pm 23$  nm in diameter resulted in large softening with a drop in hardness of 157 HV, and the advanced stage of carbide growth is the result of the high heat input from the arc welding process. On the contrary, the average carbide size at the SC-HAZ of DP980 upon RSW resulted in  $62 \pm 11$  nm with a drop in hardness of 60 HV, clearly influenced by the rapid thermal cycle.
2. The rate of softening was quantified by measuring the progression between furnace heat treatment with and without an isothermal hold at various temperatures. The predicted hardness was in good agreement with the measured hardness, in the range 400–700 °C.
3. By using an equivalent isothermal temperature approach, softening kinetic data from furnace heat treatments were used to estimate the hardness profile in gas metal arc welding, thus resulting in reasonable correspondence.
4. The JAMK equation and Yurioka's model were successfully used to predict the hardness profile along the heat-affected zone (both sub-critical and upper critical zones) of the gas metal arc welding of DP980 steel.

**Author Contributions:** Conceptualization-data curation, C.J.M.-G., V.H.B.-H. and E.A.L.-B.; formal analysis, C.J.M.-G. and V.H.B.-H.; investigation, C.J.M.-G., V.H.B.-H. and F.A.-H.; methodology, C.J.M.-G. and V.H.B.-H.; validation, E.A.L.-B.; writing—original draft, V.H.B.-H. and C.J.M.-G.; writing—review & editing, D.C.S., E.B. and N.Z. All authors have read and agreed to the published version of the manuscript.

**Funding:** This research was funded by Universidad Autónoma de Zacatecas and Centre for Advanced Materials Joining, University of Waterloo. Project UAZ-2021-38489.

**Institutional Review Board Statement:** Not applicable.

**Informed Consent Statement:** Not applicable.

**Data Availability Statement:** Not applicable.

**Acknowledgments:** Cecilio J. Martínez-Gonzalez wants to thank the Maestría en Ciencia e Ingeniería de los Materiales, Universidad Autónoma de Zacatecas and Centre for Advanced Materials Joining, University of Waterloo.

**Conflicts of Interest:** The authors declare no conflict of interest.

#### References

1. Keeler, S. Advanced High-Strength Steels Application Guidelines. Available online: <https://www.worldautosteel.org/projects/advanced-high-strength-steel-application-guidelines/> (accessed on 17 May 2022).
2. Ghosh, P.; Gupta, P.; Avtar, R.; Jha, B. Weldability of intercritical annealed dual-phase steel with the resistance spot welding process. *Weld. J.* **1991**, *70*, 7.
3. Marya, M.; Wang, K.; Hector, L.; Gayden, X. Tensile-Shear Forces and Fracture Modes in Single and Multiple Weld Specimens in Dual-Phase Steels. *J. Manuf. Sci. Eng.-Trans. Asme* **2006**, *128*, 287–298. [[CrossRef](#)]
4. Baltazar Hernandez, V.H.; Panda, S.K.; Okita, Y.; Zhou, N.Y. A study on heat affected zone softening in resistance spot welded dual phase steel by nanoindentation. *J. Mater. Sci.* **2009**, *45*, 1638–1647. [[CrossRef](#)]
5. Hernandez, B.V.H.; Kuntz, M.L.; Khan, M.I.; Zhou, Y. Influence of microstructure and weld size on the mechanical behaviour of dissimilar AHSS resistance spot welds. *Sci. Technol. Weld. Join.* **2013**, *13*, 769–776. [[CrossRef](#)]
6. Khan, M.I.; Kuntz, M.L.; Zhou, Y. Effects of weld microstructure on static and impact performance of resistance spot welded joints in advanced high strength steels. *Sci. Technol. Weld. Join.* **2013**, *13*, 294–304. [[CrossRef](#)]
7. Saha, D.C.; Westerbaan, D.; Nayak, S.S.; Biro, E.; Gerlich, A.P.; Zhou, Y. Microstructure-properties correlation in fiber laser welding of dual-phase and HSLA steels. *Mater. Sci. Eng. A* **2014**, *607*, 445–453. [[CrossRef](#)]
8. Westerbaan, D.; Parkes, D.; Chen, D.; Biro, E.; Goodwin, F.; Zhou, Y.; Nayak, S.S. Effects of concavity on tensile and fatigue properties in fibre laser welding of automotive steels. *Sci. Technol. Weld. Join.* **2013**, *19*, 60–68. [[CrossRef](#)]
9. Li, J.; Nayak, S.S.; Biro, E.; Panda, S.K.; Goodwin, F.; Zhou, Y. Effects of weld line position and geometry on the formability of laser welded high strength low alloy and dual-phase steel blanks. *Mater. Des.* **2013**, *52*, 757–766. [[CrossRef](#)]
10. Xu, W.; Westerbaan, D.; Nayak, S.S.; Chen, D.L.; Goodwin, F.; Biro, E.; Zhou, Y. Microstructure and fatigue performance of single and multiple linear fiber laser welded DP980 dual-phase steel. *Mater. Sci. Eng. A* **2012**, *553*, 51–58. [[CrossRef](#)]

11. Xia, M.; Biro, E.; Tian, Z.; Zhou, Y.N. Effects of Heat Input and Martensite on HAZ Softening in Laser Welding of Dual Phase Steels. *ISIJ Int.* **2008**, *48*, 809–814. [[CrossRef](#)]
12. Prijanovič, U.; Prijanovič Tonkovič, M.; Trdan, U.; Pleterski, M.; Jezeršek, M.; Klobčar, D. Remote Fibre Laser Welding of Advanced High Strength Martensitic Steel. *Metals* **2020**, *10*, 533. [[CrossRef](#)]
13. Burns, T.J. *Weldability of a Dual-Phase Sheet Steel by the Gas Metal Arc Welding Process*; UWSpace: Waterloo, ON, Canada, 2010.
14. Kapustka, N.; Conrardy, C.; Babu, S.; Albright, C. Effect of GMAW Process and Material Conditions on DP 780 and TRIP 780 Welds. *Weld. J.* **2008**, *87*, 135s–148s.
15. Elliot Biro, C.J.; Lyttle, K. Correlation between Failure Location and Tensile Strength of AHSS GMAW Lap Joint. In Proceedings of the Sheet Metal Welding Conference XIII, Livonia, MI, USA, 14–16 May 2008.
16. Conrardy, N.K.; Albright, C.E. Effect of material and GMAW process conditions on AHSS welds. In Proceedings of the Sheet Metal Welding Conference XII, Livonia, MI, USA, 9–12 May 2006.
17. Biro, A.L. Welded Properties of Various DP600 Chemistries. In Proceedings of the Sheet Metal Welding Conference XI, Sterling Heights, MI, USA, 11–14 May 2006.
18. Shome, M.; Tumuluru, M. Introduction to welding and joining of advanced high-strength steels (AHSS). In *Welding and Joining of Advanced High Strength Steels (AHSS)*; Woodhead Publishing: Sawston, UK, 2015; pp. 1–8. [[CrossRef](#)]
19. Duchet, M.; Haouas, J.; Gibeau, E.; Pechenot, F.; Honecker, C.; Munier, R.; Weber, B. Improvement of the fatigue strength of welds for lightweight chassis application made of Advanced High Strength Steels. *Procedia Struct. Integr.* **2019**, *19*, 585–594. [[CrossRef](#)]
20. Baltazar-Hernández, V.H.; López-Baltazar, E.A.; Alvarado-Hernández, F.; Gómez-Jiménez, S.; Ruiz-Mondragón, J.J.; Biro, E.; Zhou, N. Surface Residual Stress Analysis in GMAW and LBW of the Dissimilar TRIP-DP Steels Joint: An Experimental Approach. *Metals* **2022**, *12*, 880. [[CrossRef](#)]
21. John, M.; Kumar, A.; Bhat, U. AHSS welding using undermatching filler wires and process advantages with P-GMAW. *Mater. Today Proc.* **2022**, *49*, 1312–1318. [[CrossRef](#)]
22. Baltazar Hernandez, V.H.; Panda, S.K.; Kuntz, M.L.; Zhou, Y. Nanoindentation and microstructure analysis of resistance spot welded dual phase steel. *Mater. Lett.* **2010**, *64*, 207–210. [[CrossRef](#)]
23. Nayak, S.S.; Baltazar-Hernandez, V.; Zhou, Y. Effect of Chemistry on Nonisothermal Tempering and Softening of Dual-Phase Steels. *Metall. Mater. Trans. A* **2011**, *42*, 3242–3248. [[CrossRef](#)]
24. Gould, J.; Khurana, S.P.; Li, T. Predictions of Microstructures When Welding Automotive Advanced High-Strength Steels—A Combination of Thermal and Microstructural Modeling can be Used to Estimate Performance of Welds in Advanced High-Strength Steels. *Weld. J.* **2006**, *85*, 111S–116S.
25. Vignier, S.; Biro, E.; Hervé, M. Predicting the hardness profile across resistance spot welds in martensitic steels. *Weld. World* **2014**, *58*, 297–305. [[CrossRef](#)]
26. Biro, E.; McDermid, J.; Vignier, S.; Zhou, Y. Decoupling of the softening processes during rapid tempering of a martensitic steel. *Mater. Sci. Eng. A* **2014**, *615*, 395–404. [[CrossRef](#)]
27. Biro, E.; Vignier, S.; Kaczynski, C.; McDermid, J.; Lucas, E.; Embury, J.; Zhou, N. Predicting Transient Softening in the Sub-Critical Heat-Affected Zone of Dual-Phase and Martensitic Steel Welds. *ISIJ Int.* **2013**, *53*, 110–118. [[CrossRef](#)]
28. Biro, E.; McDermid, J.; Embury, J.; Zhou, Y. Softening Kinetics in the Subcritical Heat-Affected Zone of Dual-Phase Steel Welds. *Metall. Mater. Trans. A* **2010**, *41*, 2348–2356. [[CrossRef](#)]
29. E. Biro, A.L. Tensile properties of Gleeble simulated HAZ from various dual-phase steels. In Proceedings of the Sheet Metal Welding Conference XII, Livonia, MI, USA, 9–12 May 2006.
30. Martínez-González, C.J.; López-Ibarra, A.; Haro-Rodríguez, S.; Baltazar-Hernandez, V.H.; Nayak, S.S.; Zhou, Y. Effects of holding time on haz-softening in resistance spot welded dp980 steels—Erratum. *MRS Online Proc. Libr. Arch.* **2013**, *1485*, 1. [[CrossRef](#)]
31. RWMA. *Resistance Welding Manual*, 4th ed.; American Welding Society (AWS): Miami, FL, USA, 2003.
32. American Welding Society. *Recommended Practices for Test Methods for Evaluating the Resistance Spot Welding Behavior of Automotive Sheet Steel Materials*; American Welding Society: Miami, FL, USA, 1997.
33. Yurioka, Y.O.M.; Kasuya, T.; Cotton, H.J.U. Prediction of HAZ hardness of transformable steels. *Met. Constr.* **1987**, *19*, 217R–223R.